TECHNICAL ARTICLE

Experimental Analyses into Dry Ultrasonic Vibration-Assisted Grinding of Difficult-to-Machine Tool Steel with Alumina Wheel

Abhimanyu Chaudhari, Ashwani Sharma, Mohd Zaheer Khan Yusufzai, and Meghanshu Vashista

This paper describes experimental studies that were carried out to assess the enhancement in grinding productivity of AISI D2 tool steel by adopting the ultrasonic vibration-assisted dry grinding (UVADG) mode. Experimental works were conducted on a UVADG setup that was indigenously developed and manufactured. The grinding productivity in the UVADG mode was assessed by comparing the grinding forces, force ratio, surface roughness, bearing area curve (BAC), BAC ratio, ground surface morphology, and topography achieved in conventional dry grinding (CDG) and conventional wet grinding (CWG) modes. The UVADG mode at optimized amplitude and frequency results in lesser grinding forces and better surface integrity than CDG and CWG modes. With UVADG mode, the impact of overlapping induced by ultrasonic vibration resulted in a higher BAC ratio (88.71%) and a steeper BAC. This BAC ratio reflects the ground surface in UVADG mode, which is less susceptible to antifriction and antiwear characteristics than CDG and CWG modes. The experimental outcomes revealed that the UVADG mode has a greater potential for improving the grindability of AISI D2 tool steel. The current study also promotes the need for a sustainable grinding method for "difficult-to-machine" materials adopting UVADG mode.

1. Introduction

AISI D2 tool steel is a vital material for high caliber industrial applications, namely molds, punches, dies, commercial cutting tools, gauges, components of machinery susceptible to wear, injection screws, aerospace, automobile sectors, healthcare instruments, construction, and fabrication equipment (Ref 1, 2). This is because of its exceptional qualities, which include excellent temperature resistance, wear resistance, compressive strength, close tolerances, and a greater strength-to-weight ratio (Ref 3). Moreover, the fabricated components need significant dimensional and geometrical precision, which necessitates the use of a grinding process. Conventional dry grinding (CDG) is commonly used because of its low cost, environmental friendliness, and no use of lubricants. Furthermore, it has significant drawbacks, including thermal damage, large frictional force, high residual stress, and lower grinding

Abhimanyu Chaudhari, Ashwani Sharma, Mohd Zaheer Khan Yusufzai, and **Meghanshu Vashista**, Department of Mechanical Engineering, Indian Institute of Technology (Banaras Hindu University), Varanasi, Uttar Pradesh, India. Contact e-mail: mvashista.mec@iitbhu.ac.in.

ratio (Ref 4). Furthermore, thermal adversity has an impact on the surface integrity of the ground component. For example, Sinha et al. (Ref 5) showed that CDG caused a grinding burn area with oxidation and scratches marks. Mao et al. (Ref 6) reported that during CDG of 1045 steel using an alumina abrasive wheel, the material surface's metallographic structure was modified due to thermal damage, and the states of the samples were classified depending on the effects brought about by changes in the metallographic structure of the samples. Therefore, other methods must be explored. Although conventional wet grinding (CWG) seems to have addressed the abovementioned issues, it has created health, environmental, and economic problems (Ref 7, 8). The cutting flood removes the heat from the grinding zone. Even so, it has not always been proven to be effective. Secondly, it uses a large quantity of cutting flood: 8 L per minute (Ref 9), causing severe economic and environmental sustainability concerns. Also, current environmental laws, such as ISO 14000, have become more rigid in encouraging green manufacturing standards. This perplexing situation led to the development of novel, eco-friendly, and efficient methods, such as ultrasonic vibration-assisted dry grinding (UVADG). Ultrasonic vibration-assisted grinding is a composite technique that involves conventional grinding with ultrasonic vibration, and it has been used to produce an efficient and sustainable grinding process for materials that are "difficult to machine," namely nickel-based superalloys (Ref 10), titanium alloys (Ref 11), tool steels (Ref 12), composites (Ref 13), and ceramics (Ref 14) due to the superior surface integrity, lower grinding forces, and lower heat generation. Badiger et al. (Ref 15) established the correlation between machining parameters with cutting force, tool wear, surface roughness and built the mathematical models for cutting force and surface roughness (Ref 16); they also studied the wear surface morphology

(Ref 17), surface topography, and crystal phase (Ref 18). In most UVADG setups, ultrasonic vibrations with low amplitude (2-30 μm) and high frequency (16-40 kHz) are superimposed on the grinding wheel or the workpiece in the longitudinal or transverse direction of the table feed rate (Ref 19, 20). The effectiveness of ultrasonic grinding is substantially greater when vibration is superimposed on the workpiece owing to changes in mechanical characteristics of the material, such as decreases in yield points, strength, and resistance to plastic deformation (Ref 21). It was reported that the UVADG of carbon steel displayed the highest decrease of 20% in surface roughness compared to the CDG and the readings of the Abbott–Firestone curve's indices, i.e., heights of the peaks (R_{pk}), valleys (R_{vk}), and core roughness (R_k) under UVADG, were lower as compared to CDG. (Ref 22). Another study found that the UVADG could considerably increase the surface bearing and the fluid retention characteristics of the ground component (Ref 23). Reduced coefficient of friction on the tool–workpiece interface and shearing layers inside the finished material and material softening because of confined localized heat induced by ultrasonic vibration at the interface region of the tool–workpiece resulting in the more effortless relative motion of them (Ref 24). In a previous study, the frequency and amplitude of ultrasonic vibrations were shown to substantially impact the grinding force, surface morphology and surface roughness, and low amplitude and high frequency were shown to promote superior surface integrity (Ref 25). Specifically, Mult et al. (Ref 26) reported that using vertical ultrasonic grinding caused a modest increase in wheel wear because the grinding wheel struck the ground workpiece. Furthermore, among the essential fundamental characteristics to explain the grinding mechanism is the grinding force, which represents the contact among the abrasive grits and the work material in the machining region and is closely associated with the material removal mechanism in the grinding operation and the quality of the ground surface (Ref 27). As a result, analysis of grinding force continues to be a significant way of understanding the mechanism of ultrasonic vibration-assisted grinding. According to Zhang et al. (Ref 28), the average cutting velocity in ultrasonic grinding was greater than that in conventional grinding, which is the crucial reason leading to the decrease in grinding forces. Since ultrasonic vibration-assisted grinding could decrease grinding force and achieve better integrity when the vibration direction is tangential to the workpiece, previous research revealed that the primary function was to reduce grinding chip volume owing to the interaction of abrasive grits path (Ref 29). As theoretically, the interaction mechanism, referred to as the ultrasonic vibration impact, is primarily governed by the grinding and vibration parameters of a particular grinding wheel. Moreover, the research (Ref 21, 24, 30) revealed that ultrasonic-assisted grinding could achieve almost the same decrease in grinding force and ground surface roughness, even when the grinding parameters had been substantially different, whereas vibration parameters remained constant. Thus, it is worth addressing whether UVADG mode can consistently provide outstanding performance over such a varied range of grinding and vibration parameters.

Therefore, the present research focuses on improving the grinding performance of AISI D2 tool steel by examining the influence of grinding parameters on UVADG mode and comparing it to CDG and CWG modes. The downfeed and vibration amplitude were varied throughout the test, while the grinding speed, worktable feed rate, and ultrasonic frequency

stayed unchanged. The bearing area curve (BAC) and BAC ratio were computed using the three-dimensional roughness parameters in order to determine the best antifriction and antiwear properties of the ground workpiece. Since the current study correlates to "difficult-to-machine" materials, namely AISI D2 tool steel, an advantage of UVADG on the grinding forces, force ratio, surface integrity, antifriction, and antiwear characteristics parameters are of importance for engineering application. These parameters have been established through this work, which is the unique novelty of this present work, and it offers an improvement of our understanding of ultrasonic vibration-assisted dry grinding of "difficult-to-machine" steels, namely AISI D2 tool steel.

2. Experimental Details

As demonstrated in Fig. 1(a), the precision surface grinding machine (maker: HMT Limited, Model: H-455) combined with the coolant and lubrication system was used to conduct grinding experiments. The grinding wheel (maker: Carborundum) was made of white alumina and had the following manufacture specifications: "AA-60-K-5-V-6." The diameter, bore, and width of the grinding wheel was 250, 76.2, and 20 mm. Each experiment group was conducted in plunge grinding mode settings for 12 passes with repetition three times to minimize the random test errors, and the average value was computed. After each group grinding operation, the grinding wheel was dressed with a one carat single point diamond dresser to ensure all the experiments were consistent, and dressing parameters are listed in Table 1. Based on preliminary tests, four downfeed (10, 20, 30, and 40 μm), wheel velocity (39.42 m/s), and table feedrate (9 mm/min) were chosen for grinding AISI D2 tool steel workpiece (dimension: $80^L \times 10^T \times 15^W$ mm). All workpieces underwent heat treatment at an outdoor heat treatment facility (maker: Metals Heat Treatment, India) to achieve an industrial application-based hardness of 58 $\pm$ 2 HRC. Firstly, each workpiece was preheated slowly up to 650 °C and held until uniform heating of each workpiece and then continued heating till 1050 °C for 90 min in the vacuum furnace (maker: SECO-WARWICK, India), and then cooled in oil quench. The electrical power source for this furnace was 230 V and 50 Hz, and the quenching pressure was kept between 5 and 8 bar. The vacuum furnace's technical specifications are working zone size: $610 \times 750 \times 1000$ mm, maximum temperature: 1250 °C, and load grass mass: 1000 kg. Finally, workpieces were primary tempered at 400 °C for 120 min and secondary tempered at 450 °C for 120 min to relieve internal stresses due to quenching. The x-ray fluorescence (XRF) spectroscopy (maker: Bruker, model: S4 Pioneer) was used to determine the elemental composition of the workpiece material, as shown in Table 2. The tangential and normal grinding forces were measured using a three-dimensional grinding force dynamometer (make: IEICOS-India, Model: 3 Channel-610C) with a sampling rate 1000 Hz, a frequency filter range of 0-45 kHz, and a response time of one millisecond. Dynamic grinding force software was used to filter the grinding force signals. The workpiece was fastened into the workpiece holding fixture before being placed on the dynamometer. The indigenously developed UVADG setup was calibrated before performing the tests using a standard method for grinding force computation
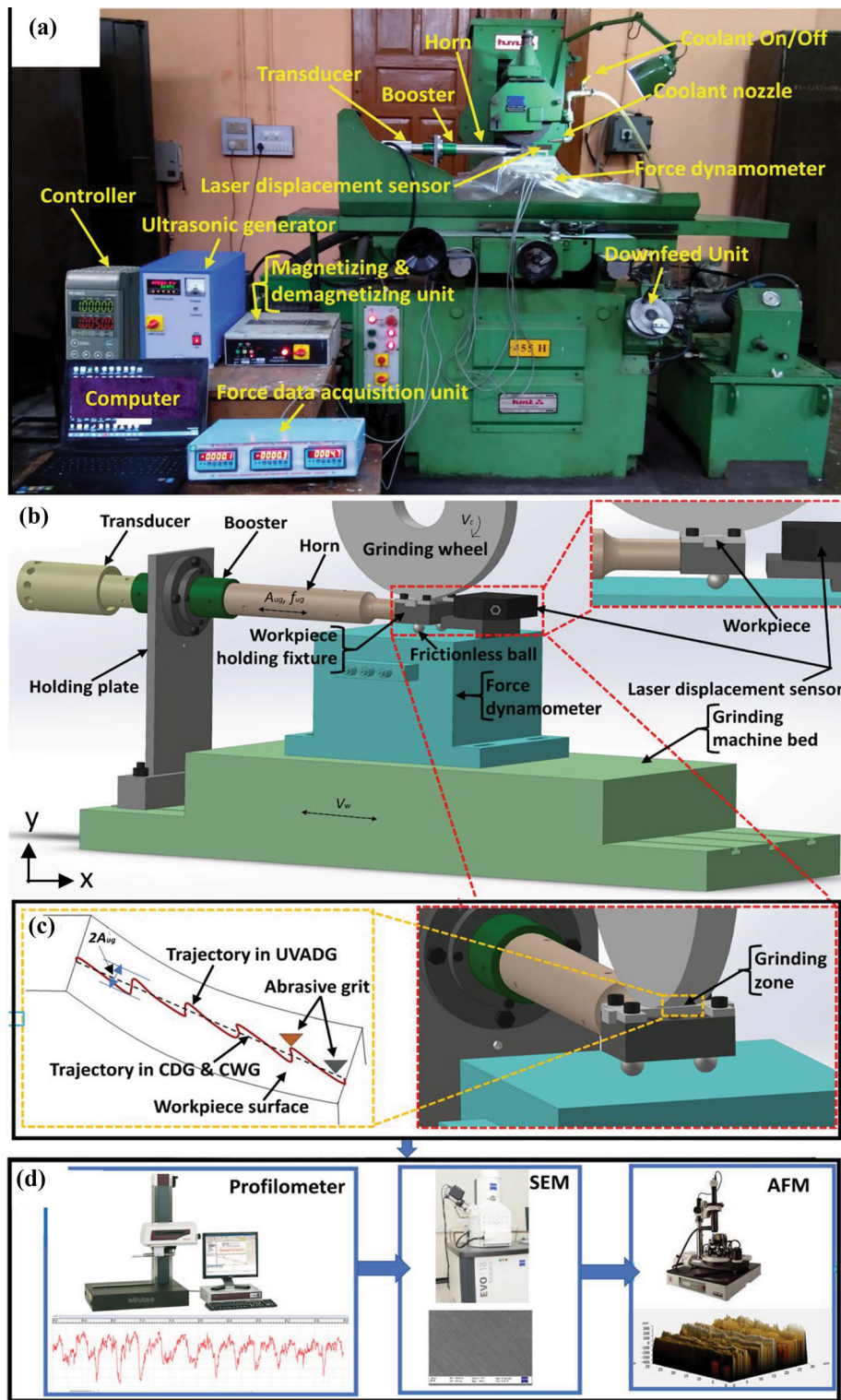
Fig. 1 The experimental setup for surface grinding: (a) actual experimental setup for UVADG, (b) schematic of 3D UVADG setup, (c) grinding zone and trajectory of abrasive grit, and (d) surface characteristics measuring instrument

based on standard procedure. The UVDAG system components are shown in detail in Fig. 1(a): actual experimental setup for UVADG and Fig. 1(b): schematic of the 3D UVADG setup. The supplied electrical energy (50Hertz) to the ultrasonic generator (maker: Ultra Autosonic India) was first transformed into mechanical vibration of 21 kHz via a piezoelectric

transducer. The ultrasonic transducer then delivers ultrasonic tangential vibration at the matching frequency. After that, the tangential vibration was subsequently amplified with a booster and a titanium horn. The workpiece holding fixture was joined with the titanium horn and kept on the force dynamometer by two supporting frictionless balls to diminish the vibration loss.

Table 1 Parameters settings for grinding

Parameters	Conditions
Grinding type	Plunge surface grinding
Grinding modes	Conventional dry grinding (CDG),
	Conventional wet grinding (CWG),
	Ultrasonic vibration-assisted dry grinding (UVADG)
Cutting fluid	Water-based soluble oil (Cimtech-D14)
Grinding wheel specification	AA-60-K-5-V-6
Workpiece material	AISI D2 tool steel
Wheel speed (V_c)	39.42 m/s
Worktable feed rate (V_w)	9 m/min
Downfeed (a_p)	10-40 μm
Ultrasonic frequency (f_{ug})	21 kHz
Vibration amplitude (A_{ug})	4-10 μm
Dresser	Single point diamond
Dressing down feed	50 μm in 8 passes
Dressing feed	180 mm per min

Table 2 Chemical composition of the AISI D2 tool steel (wt.%)

Elements	C	Cr	Si	Mn	Mo	V	Fe
Weight, %	1.55	11.80	0.30	0.40	0.90	0.80	Balance

The tangential vibration amplitudes on the workpiece were controlled, varied, and measured with the help of laser displacement sensor and controller (maker: Keyence, Model: LK-G32). This experiment used the same setup for UVADG, CDG, and CWG modes to carry out the tests. In the CWG mode, the cone-shaped nozzle with a 10 mm output diameter was used to provide twenty percent water-based cutting fluid to the grinding zone at a flow rate of 1.5 L per minute. However, during conventional grinding, ultrasonic power was shut down. The ground workpiece was cleaned in an ultrasonic bath with ethanol for 10 min following the grinding operations. A 2D surface profilometer (maker: Mitutoyo, Model: SV-2100-S4) was utilized to measure the surface roughness (R_a and R_z) at three distinct places on the ground surface perpendicular to the grinding plane.

An algorithm called a low-pass Gaussian filter was used to get the average line roughness out of the raw profile having traverse length (4 mm) and cutoff length (0.8 mm). For surface morphology and topography analysis, all ground workpieces were sliced perpendicular to the ground surface using wire electrical discharge machining (maker: Medha Ent, model: Expresscut-Ex4032C) in a square shape (dimension: 10 × 10 mm) to prevent thermal damage to the workpiece while the cutting process. Furthermore, the morphology of the ground workpiece was analyzed using the scanning electron microscope/SEM (maker: Zeiss, model: EVO-18-Research). The nanoscale 3D surface topography and bearing area curve parameters values of the ground workpiece were obtained using an atomic force microscope/AFM (maker: NT-MDT, Model: NTEGRA PRIMA), as shown in Fig. 1(d).

As demonstrated in Fig. 1(c), the trajectory of conventional grinding is linear, while ultrasonic grinding pursues a sine waveform trajectory due to the ultrasonic vibration on the workpiece. The direction of ultrasonic vibration is tangential to the worktable feed rate. The ultrasonic vibration-assisted grinding process has a periodic reciprocating motion, which results in the discontinuous cutting action of abrasive grits. The velocity component of the abrasive grain under a UVADG mode can be shown mathematically from Eq 1 and 2:

$$V_x = (-1)^n \times V_w + V_c \times \cos(\omega_c \times \tau) \\ + 2\pi f_{ug} \times A_{ug} \cos(2\pi f_{ug} \tau + \beta_0) \tag{Eq 1}$$

$$V_y = V_c \times \sin(\omega_c \times \tau) \tag{Eq 2}$$

where $n = 0$ for down grinding and $n = 1$ for up grinding. Further, V_x and V_y are the horizontal and vertical components of abrasive grain velocity in UVADG at time τ. The ultrasonic vibration amplitude is A_{ug}, and the vibration frequency is f_{ug}. The grinding wheel's linear and angular speeds are V_c and ω_c. The worktable feedrate V_w and initial phase angle β_0.

The standard procedure was used in this work as follows. We have calibrated the ultrasonic vibration-assisted grinding setup for grinding force measurement. Supplementary Fig. 1(a) shows that ultrasonic vibration is off without putting a 5 kg load on the workpiece, and the force data acquisition unit displays zero grinding force reading. Besides, Supplementary Fig. 1(b) shows that ultrasonic vibration is off with just slowly putting a 5 kg load over the workpiece, and the force data acquisition unit displays a 5kgf ($\sim$ 50 N) normal grinding force reading, which indicates that the proper design and develop an ultrasonic vibration-assisted grinding setup for assessment of grindability and surface integrity of AISI D2 tool steel.

3. Result and Discussion

3.1 Grinding Forces

In the grinding domain, grinding force is a critical parameter to characterizse the grinding process because it helps estimate the grinding force ratio, grinding wheel life, surface roughness, and grinding temperature (Ref 31). Figure 2(a) and (b) depicts the change of tangential (F_c) and normal (F_p) grinding force computed during each pass for CDG, CWG and UVADG (at A_{ug} = 4, 7 and10μm) modes at 10 μm and 40 μm downfeed. Each set of experiments in this investigation follows the same
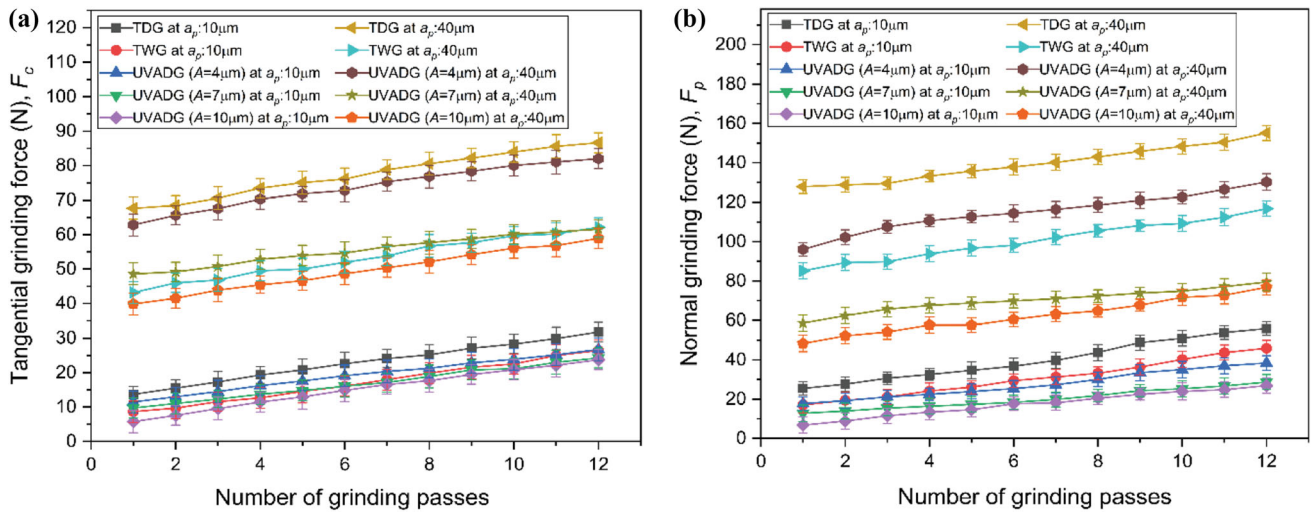
Fig. 2 Variation of grinding forces (a) tangential and (b) normal, with number of passes at downfeed of 10 and 40 μm under different modes

pattern. As shown in Fig. 2(a) and (b), owing to the expected interaction of mostly negatively raked abrasives present in the abrasive wheel's edge, normal grinding force components are always higher than the tangential grinding force.

The UVADG (at A_{ug} = 10 μm) mode can reduce the F_c and F_p compared with CDG and CWG modes under the same conditions. In addition, both the grinding forces during CDG, CWG, and UVADG modes increase along with the increasing grinding passes. This may be due to the wear out of the grinding wheel grits with the increase in the grinding passes. Ding et al. (Ref 32) found an increase in grinding force with a number of passes while ultrasonic vibration grinding of silicon carbide. Also, the grinding forces were higher with the rise in downfeed in all grinding modes. An increase in downfeed at constant wheel speed led to increased maximum uncut chip thickness or wheel loading because of the increased friction between the abrasive wheel and ground surface interface. In case of UVADG, the material removal mechanism is varied due to the characteristic of separability. The cutting process becomes discontinuous because of the high-frequency interaction between active abrasive grits and the ground surface. Therefore, the grinding forces increase relatively slowly during UVADG (A_{ug} = 10 μm) with increasing the number of grinding passes compared with CDG and CWG modes. As presented in Fig. 2(a) and (b), during the first pass, the F_c obtained in UVADG (A_{ug} = 10 μm) mode was decreased by 41.06, 13.26, 26.56, and 17.96% as compared to CDG, CWG, UVADG (A_{ug} = 4 μm), and UVADG (A_{ug} = 7 μm) modes, and F_p was reduced by 62.23, 43.28, 49.73, and 17.62% as compared to CDG, CWG, UVADG (A_{ug} = 4 μm), and UVADG (A_{ug} = 7 μm) modes, respectively. While during the 12th pass, the F_c and F_p increased to 31.97 and 50.51% in CDG mode, 8.54 and 34.25% in CWG mode, 28.12 and 41.06% in UVADG (A_{ug} = 4 μm), and 4.31 and 3.34% in UVADG (A_{ug} = 7 μm) as compared to UVADG (A_{ug} = 10 μm) mode. As a result, it can be concluded that adopting UVADG modes makes it considerably easier to keep the grinding wheel sharp.

The standard deviation of ground forces is illustrated by the error bar. Figure 3 depicts the grinding forces under CDG, CWG, and UVADG (at A_{ug} = 4, 7, 10 μm) modes at downfeed of 10, 20, 30, and 40 μm, respectively, while worktable feed

rate was 9 m/min. The grinding forces were computed without the forces for the first five passes to skip the inconsistencies involved with eliminating the relative stiffness. The normal component of grinding force denotes the ease with which material can be removed due to abrasive penetration on the substrate surface. On the other hand, the tangential component denotes the ease with which material can be removed during shearing action, which is preferred to be the better effective reason for material removal.

As shown in Fig. 3(a) and (b), the lowest F_c and F_p were found under UVADG (at A_{ug} = 10 μm) at respective downfeed with corresponding CDG and CWG modes. In the case of CDG mode, because of the ploughing and rubbing action of the abrasive wheel on the workpiece surface (refer to Fig. 7) in the absence of coolant and lubrication, larger grinding forces (F_c and F_p) were generated in the machining zone. While the coolant in the CWG mode can advance toward the elastic grinding region, it is hard to approach the plastic grinding region owing to the hydrodynamic boundary layer forming around the abrasive wheel's periphery (Ref 33). As a result, the coolant has a cooling impact on a smaller area of the ground sample, which increases the grinding forces. In UVADG mode, on increasing the vibration amplitude from A_{ug} = 4 μm to A_{ug} = 10 μm, the more effective is the influence of the engaged abrasive grits on the ground sample. The grinding zone generates an effective interaction between abrasive grits and the sample surface due to the discontinuous kinematics of the cutting process in ultrasonic grinding, allowing the material to begin removing more effectively. Therefore, frictional impact (refer to Fig. 4) and F_c and F_p are reduced, resulting in very little plastic deformation (refer to Fig. 7) occurs in UVADG.

3.2 Force Ratio

The grinding force ratio is an important parameter in finishing operations because it offers quantitative information about the productivity of the grinding process. The ratio of tangential to normal grinding force can be used to calculate the friction coefficient (μ) or grinding force ratio. Due to its similarity to a coefficient of friction, the same symbol, μ, is used (Ref 34):
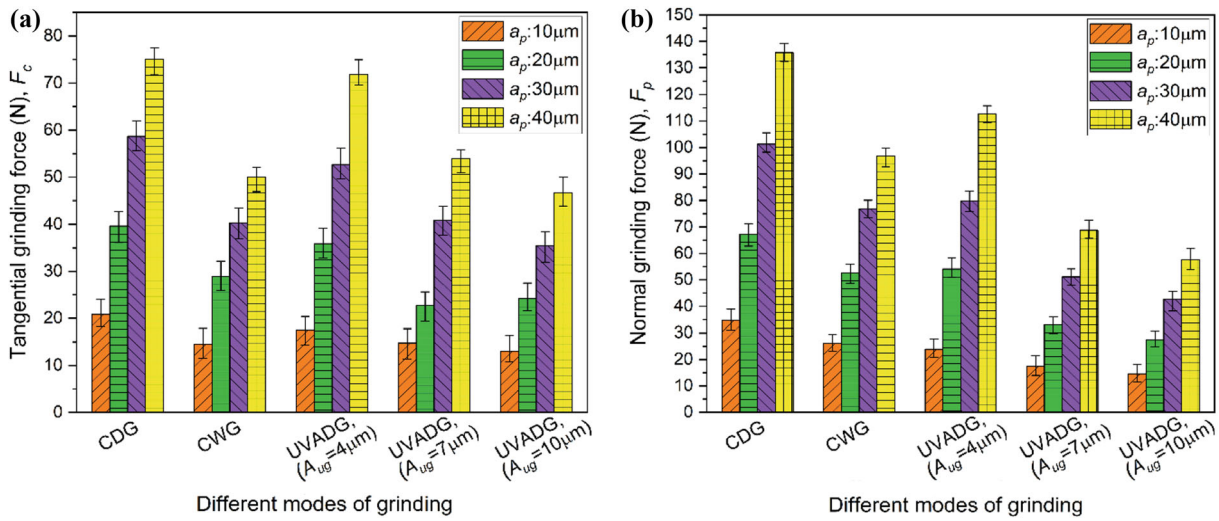
Fig. 3 Variation of grinding forces (a) tangential and (b) normal under different modes
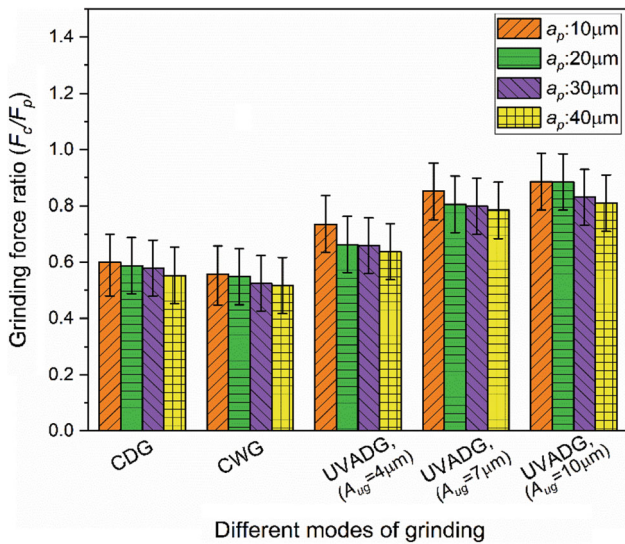

Fig. 4 Change of grinding force ratio in various grinding modes

$$\mu = \frac{F_c}{F_p}$$

Figure 4 shows the variation in the F_t/F_n ratio under the CDG, CWG, and UVADG (at A_{ug} = 4, 7, 10 μm) modes at downfeed of 10, 20, 30, and 40 μm. As downfeed (a_p) increased, the corresponding F_c/F_p ratio was reduced in each distinct mode of grinding. The F_c/F_p ratio was seen to differ in the span of 0.5164 to 0.8863 under CDG (at a_p = 40 μm) and UVADG (at a_p = 10 μm), respectively. The F_c/F_p ratios in CWG, CDG, UVADG (at A_{ug} = 4 μm), and UVADG (at A_{ug} = 7 μm) grinding mode were 0.5164, 0.5531, 0.6357, and 0.7852, respectively, which were 35.12, 32.43, 22.29, and 4.10% smaller than that of UVADG (at A_{ug} = 10 μm). A high F_c/F_p ratio implies a sharper grinding wheel, while a low F_c/F_p ratio means dull grinding wheel (Ref 35). The UVADG mode provides a higher F_c/F_p ratio, indicating that the decrease in F_p was more significant than F_c. UVADG generates a self-sharpening tendency of the abrasive wheel to maintain the

sharp edges of abrasive grits (Ref 36). The sharp edges of abrasive grits caused more intense penetration into the work surface, reducing grinding forces.

3.3 Surface Roughness

The small variable grooves and tiny peaks–valleys on the ground workpiece created by randomly distributed alumina grits and substantial plastic deformation are used to measure surface roughness (Ref 37). The R_a and R_z parameters are extensively used in precision manufacturing industries for period bearing area analysis, which provides qualitative information regarding wear resistance of ground sample (Ref 38). The influence of different grinding modes and downfeed on surface roughness indices such as R_a and R_z is shown in Fig. 5. When the downfeed was increased, both R_a and R_z values gradually increased, regardless of the grinding mode used. This might be due to a rise in the number of active grits per unit cross-sectional area as downfeed increases. Fracture and pull-out from the bonding agent are caused by these grits. As a result, as the grit spacing increases, the peak to valley roughness profile becomes larger at greater downfeed.

The maximum R_a (0.8137 μm) and R_z (4.8431 μm) values were found in CDG due to the greater rubbing and ploughing impact than CWG and UVADG (refer to Fig. 7a). The R_a values in the CWG, UVADG (at A_{ug} = 4 μm), UVADG (at A_{ug} = 7 μm), and UVADG (at A_{ug} = 10 μm) were 0.6249, 0.6734, 0.5164, and 0.4576 μm, respectively, and which were decreased by 23.20, 16.24, 35.53, and 42.76% as compared to CDG, respectively. The R_z values in the CWG, UVADG (at A_{ug} = 4 μm), UVADG (at A_{ug} = 7 μm), and UVADG (at A_{ug} = 10 μm) were 4.4277, 4.5644, 3.6825, and 3.2082 μm, respectively, and which were decreased by 7.57, 4.75, 22.96, and 34.75% as compared to CDG, respectively. Further, the span (2 A_{ug}) of the cutting furrow in ultrasonic grinding (refer to Fig. 1c) is larger as compared to the conventional grinding which results in larger grinding furrows, and relatively uniform grinding surfaces can be obtained. Therefore, the surface roughness in case of UVADG mode reduces remarkably. Also, because ultrasonic vibration grinding applies additional stress to aid in the disintegration of instantaneous welds, it reduces the amount of time that any two asperities on counter surfaces
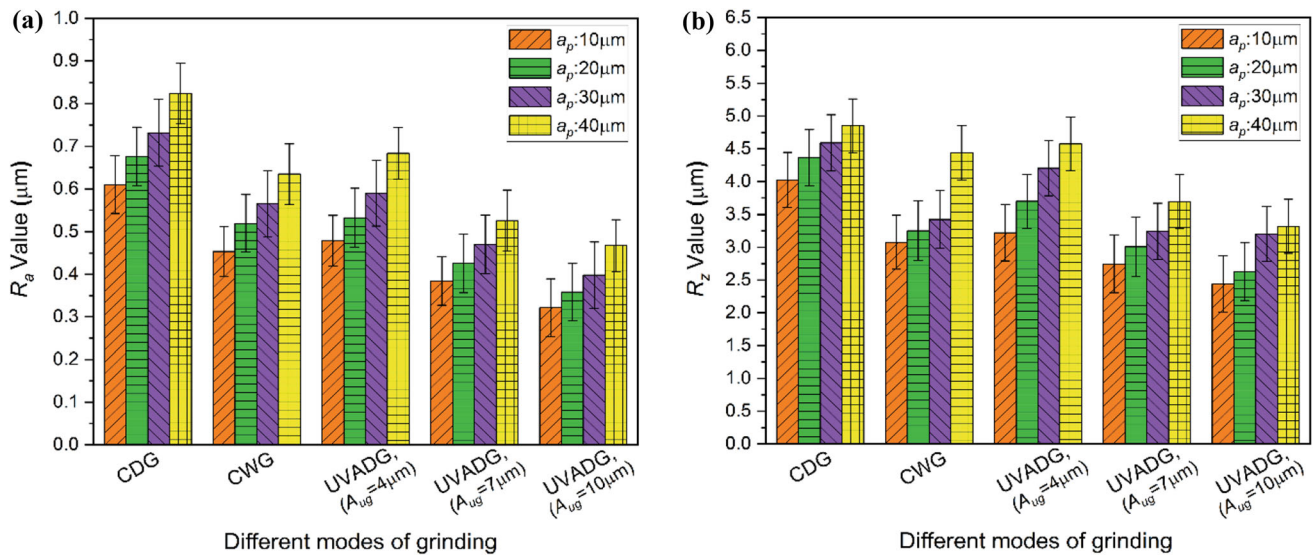
Fig. 5 Variation of (a) R_a value and (b) R_z value under different modes

may remain in temporary contact, preventing the formation of a stable weld (Ref 4). This means that with UVADG, there are fewer stable bonds established between the abrasive grits and the ground surface. As a result, the surface roughness in UVADG reduces.

3.4 Bearing Area Characteristics

The contact state of two physical surfaces is referred to as the bearing area curve (BAC), and it offers qualitative information on component wear resistance. The BAC indicates the percentage or linear fraction of a profile over a specific height. Surface roughness findings may be easier to understand if the BAC is divided into subsections, such as core roughness depth (S_k), reduced peak height (S_{pk}), and reduced valley depth (S_{vk}), which were calculated using the BAC based on the ISO 25178-2 (2012) standard (Ref 39), as shown in Fig. 6(c). A straight line based on a best-fit line across 40% of the BAC's center part can be drawn for this purpose. Furthermore, the BAC ratio (SMr2-SMr1) is expressed as a percentage area encountered by intersecting a line that divides the peak and valley profiles from the core profile. In addition to that, the peak material portion (SMr1) specifies the percentage of material that includes the S_{pk} peak structures, and the valley material portion (SMr2) refers to the percentage of the measurement area that constitutes the S_{vk} deeper valley structures. The higher BAC ratio showed that the machine parts had a larger bearing area and enhanced antifriction and antiwear characteristics (Ref 25). This research examines the BAC of various ground workpieces for a qualitative surface quality assessment in different grinding modes. Figure 6(a) and (b) illustrates the BAC and BAC ratio of the ground workpiece under CDG, CWG, and UVADG modes with varying ultrasonic vibration amplitude. In UVADG mode, a higher BAC ratio was achieved because of the impact of overlapping induced by ultrasonic vibration. The higher ultrasonic amplitude (at A_{ug} = 7 and 10 μm) can induce better evident overlapping. This might be the reason that an increase in the ultrasonic vibration amplitude generated a higher BAC ratio, which considerably prevents the rubbing activity on the ground surface. To put it another way, the core roughness profile generated a steeper BAC. The CWG mode has a nearly

identical BAC shape to the UVADG mode (at A_{ug} = 7 μm) but a slightly lower BAC ratio (refer to Fig. 6a, b) due to multiple valley points on the ground surface that affect the entire BAC. The CDG mode had the lowest BAC ratio, revealing relatively deep scratches on the ground surface due to the lack of coolant. In addition to that the reduced peak height S_{pk}, the parameter illustrating the height at which peaks rise from the core profiles gives information about the running-in process of the surface. A lower S_{pk} value corresponds to a shorter running-in phase and provides more initial contact area; therefore, there is a lower area of contact stress when the surface is contacted (Ref 22, 40). As shown in Fig. 6(a) and Table 3, the S_{pk} value of UVADG (at A_{ug} = 10 μm) is lower than that of UVADG (at A_{ug} = 7 μm), CWG, UVADG (at A_{ug} = 4 μm), and CDG, respectively. That means the running-in time and area of contact stress of the ground surface after UVADG (at A_{ug} = 10 μm) are smaller than that after UVADG (at A_{ug} = 7 μm), CWG, UVADG (at A_{ug} = 4 μm), and CDG, respectively.

Furthermore, the core roughness height of UVADG (at A_{ug} = 10 μm) is more centralised than that of UVADG (at A_{ug} = 7 μm), CWG, UVADG (at A_{ug} = 4 μm), and CDG, respectively. Hence, the core roughness depth S_k, which describes the part of the roughness profile without any peaks or valleys, is shorter in UVADG (at A_{ug} = 10 μm) than that in UVADG (at A_{ug} = 7 μm), CWG, UVADG (at A_{ug} = 4 μm), and CDG, respectively. During operation, there is high mechanical resistance, and hence, the manufacturing process is constructively controlled by providing lower S_k values (Ref 22, 40). This signifies that the bearing capacity of the finished surface after UVADG (at A_{ug} = 10 μm) is best to that after UVADG (at A_{ug} = 7 μm), CWG, UVADG (at A_{ug} = 4 μm), and CDG, respectively.

3.5 SEM and AFM Micrographs

Surface morphology and topography are a critical criterion for determining surface integrity. This index indicates the interaction of abrasive grits with the ground surface and material removal mechanism. The most efficient direct techniques for evaluating microscopic changes in finished parts are SEM and AFM. SEM (2D) and AFM (3D) micrographs of
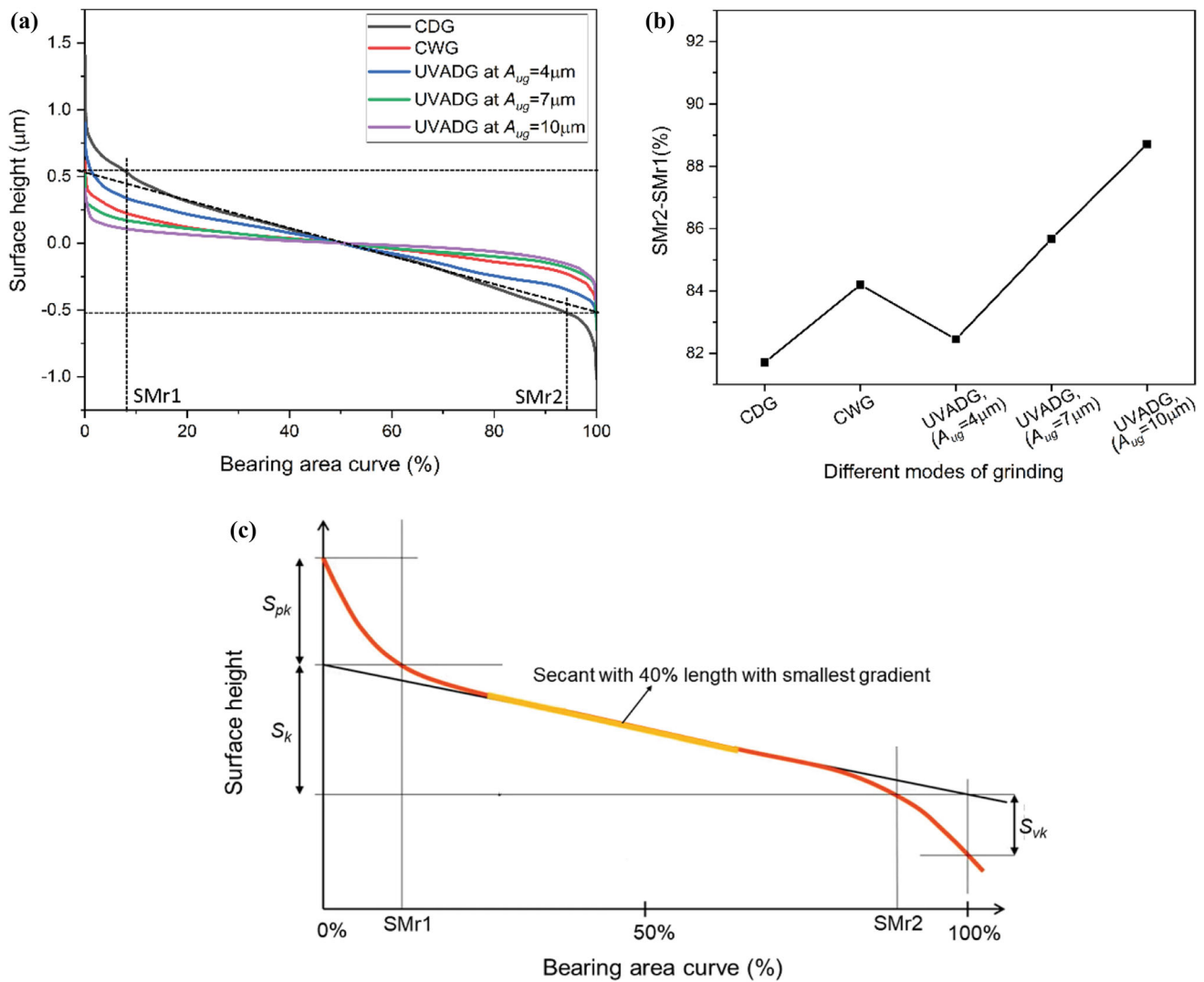
Fig. 6 Bearing area assessment under various grinding modes: (a) bearing area curve, (b) bearing area curve ratio, and (c) parameters of bearing area curve

Table 3 Parameter of bearing area curve

Mode	S_{pk}, μm
CDG	1.41
CWG	0.62
UVADG (at A_{ug} = 4 μm)	0.90
UVADG (at A_{ug} = 7 μm)	0.51
UVADG (at A_{ug} = 10 μm)	0.43

ground surface morphology and topography at 40 μm downfeed under various grinding modes are shown in Fig. 7. Deep grooves, severe ploughing, rubbing marks, and plastic deformation were noticed on the ground surface in CDG mode, as illustrated in Fig. 7(a). Also, excessive heat generation in the machining zone promotes the redeposition of the grinding material on the ground surface and compromises the surface quality of the finished component. This occurs due to prolonged abrasive grits contact with the workpiece surface, lacking a cooling and lubricating effect in CDG mode.

Owing to the low thermal conductivity of workpiece material, grinding chips clung to the wheel's abrasive grits.

Furthermore, those grinding chips were redeposited on the finished surface, resulting in ploughing, and rubbing marks on the ground component. In CWG mode, as illustrated in Fig. 7(b), minor rubbing and ploughing marks can be noticed on the ground surface owing to the insufficient strength of adsorption tribo-boundary films. However, the surface quality of the ground component was good as compared to CDG and UVADG (at A_{ug} = 4 μm) modes. On the other hand, UVADG mode produces smooth and uniform surfaces, as shown in Fig. 7(d) and (e). During UVADG mode, the workpiece surface separates from the abrasive grit within per cycle of ultrasonic vibration. Such discontinuous contact reduces the total time for heat conduction between the workpiece and abrasive grits. This decreases the heat generated in the grinding zone and wheel wear, which eventually enhances the surface quality of the ground workpiece. In several industrial applications, the surfaces of the components interacted in three dimensions. A surface roughness assessment based on a two-dimensional technique may not correctly describe a surface. Surface roughness can be more precisely determined by measuring it over an area than a line (Ref 41). The surface parameters indicated using a three-dimensional method are shown by S
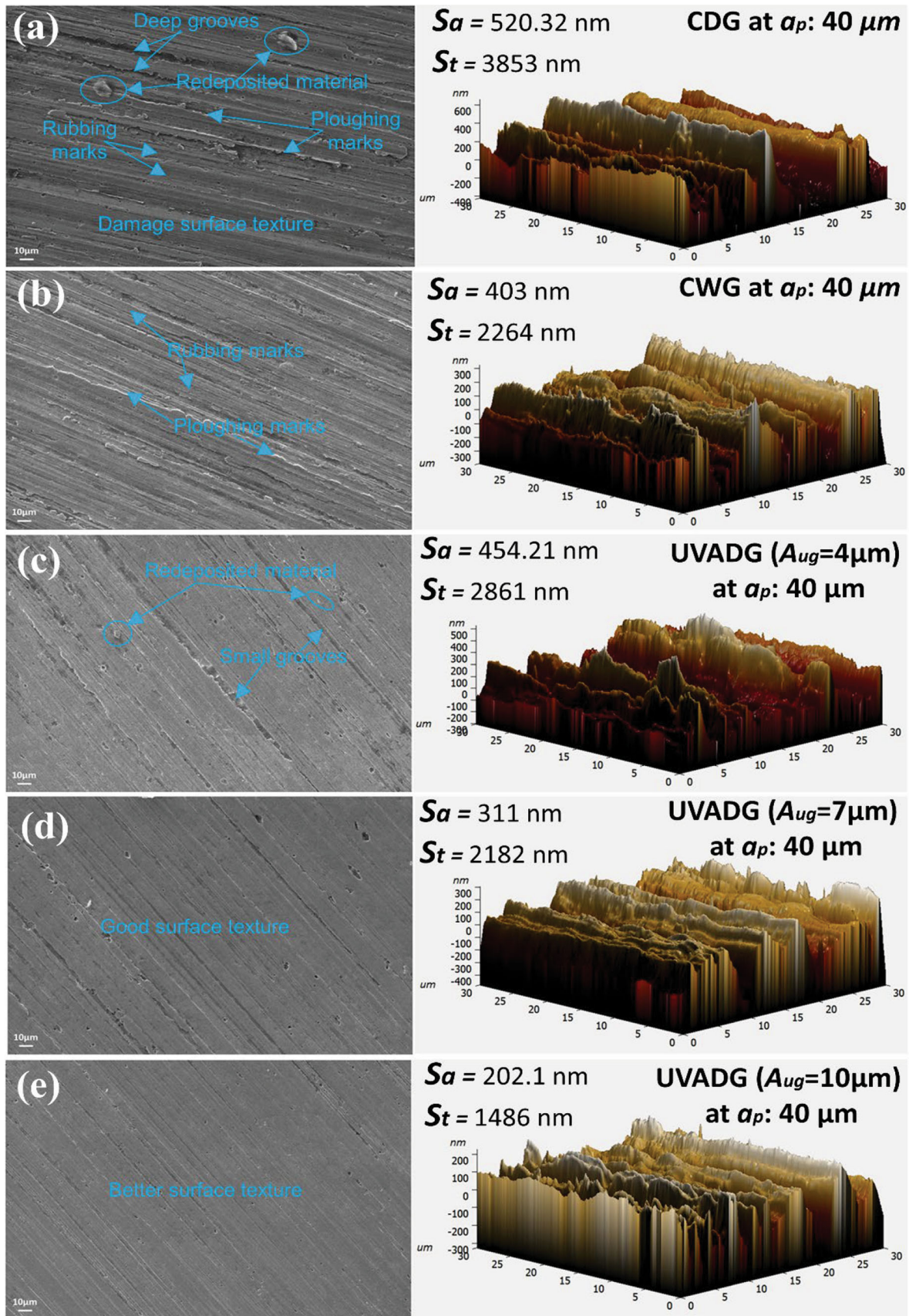
Fig. 7 SEM (2D) and AFM (3D) micrographs of ground surface morphology and topography under various grinding modes (a) CDG, (b) CWG, (c) UVADG (A_{ug} = 4 μm), (d) UVADG (A_{ug} = 7 μm), and (e) UVADG (A_{ug} = 10 μm)

instead of R. According to the AFM findings, as shown in Fig. 7, the arithmetic mean height surface roughness (S_a) value of the ground workpiece at 40 μm downfeed under CDG, CWG, UVADG (at A_{ug} = 4 μm), UVADG (at A_{ug} = 7 μm), and UVADG (at A_{ug} = 10 μm) was 520.32, 403, 454.21, 311, and 202.1 nm, respectively. The total height surface roughness (S_t) value of the ground workpiece at 40 μm downfeed under CDG, CWG, UVADG (at A_{ug} = 4 μm), UVADG (at A_{ug} = 7 μm), and UVADG (at A_{ug} = 10 μm) was 3853, 2264, 2861, 2182, and 1486 nm, respectively. These outcomes confirmed that ultrasonic vibration provided better surface roughness (refer to Fig. 7d, e).

4. Conclusion

In this experimental research work, ultrasonic vibration was implemented in the grinding of AISI D2 tool steel to illustrate the benefits of UVADG. The grinding performance was thoroughly investigated, including the grinding force and force ratio, surface roughness, bearing area curves, and ground surface quality. The following is a summary of the key conclusions:

- In terms of grinding forces, ultrasonic vibration (at A_{ug} = 10 μm) in the UVADG mode was effective in significantly decreasing grinding forces compared to CDG and CWG modes due to their intermittent cutting activity and very little plastic deformation, and smaller frictional effect.
- Because of UVADG mode grinding wheels self-sharpen, the grinding force ratio was greater than in CDG and CWG modes. A greater force ratio denotes a sharper grinding wheel, whereas a lower ratio denotes a dull grinding wheel.
- UVADG (at A_{ug} = 10 μm) mode reduces surface roughness better than CDG and CWG modes. The maximum decrease percentage of R_a and R_z in UVADG mode was 43.76 and 33.75% compared to CDG mode and 26.77 and 27.54% compared to CWG mode, respectively, at a downfeed of 40 μm.
- Ultrasonic vibration-induced overlapping resulted in a higher BAC ratio (88.71%) and a steeper BAC in UVADG mode (at A_{ug} = 10 μm). This BAC ratio represents the ground surface under UVADG mode, which has significant antifriction and antiwear characteristics.
- Compared to CDG and CWG modes, UVADG mode has provided smooth and uniform surfaces by separating the workpiece surface from the abrasive wheel during ultrasonic vibration cycles, improving ground surface quality. The S_a and S_t values also confirmed that UVADG mode provided lower surface roughness.

References

1. R. Choudhary, H. Kumar, and S. Singh, Machining Performance and Surface Integrity of AISI D2 Die Steel Machined Using Electrical Discharge Surface Grinding Process, *J. Mater. Eng. Perform.*, 2013, **22**(12), p 3665–3673. https://doi.org/10.1007/S11665-013-0679-8/FIGURES/9

2. M.A.S. Bin Abdul Rahim, M. Bin Minhat, N.I.S.B. Hussein, and M.S. Bin Salleh, A Comprehensive Review on Cold Work of AISI D2 Tool Steel, *Metall. Res. Technol.*, 2018, **115**(1), p 104. https://doi.org/10.1051/METAL/2017048

3. A. Sharma, M.Z.K. Yusufzai, and M. Vashista, A Comparative Analysis of Grinding of AISI D2 Tool Steel under Different Environments, *Mach. Sci. Technol.*, 2022 https://doi.org/10.1080/10910344.2022.2044853

4. T. Tawakoli, and B. Azarhoushang, Influence of Ultrasonic Vibrations on Dry Grinding of Soft Steel, *Int. J. Mach. Tools Manuf.*, 2008, **48**(14), p 1585–1591

5. M.K. Sinha, D. Setti, S. Ghosh, and P. Venkateswara Rao, An Investigation on Surface Burn during Grinding of Inconel 718, *J. Manuf. Process.*, 2016, **21**, p 124–133

6. H. Mao, Y. Liu, H. Mao, J. Fu, Y. Tang, and X. Li, Study for Characterizing Grinding Burn of 1045 Steel Based on Nonlinear Ultrasonic Coefficients, *J. Mater. Eng. Perform.*, 2022 https://doi.org/10.1007/S11665-022-06915-0/FIGURES/19

7. M.K. Sinha, R. Madarkar, S. Ghosh, and P.V. Rao, Application of Eco-Friendly Nanofluids during Grinding of Inconel 718 through Small Quantity Lubrication, *J. Clean. Prod.*, 2017, **141**, p 1359–1375

8. A. Chaudhari, A.S. Awale, and A.K. Chakrabarti, Surface Integrity Characterization of Austenitic, Martensitic and Ferritic Stainless Steel under Different Grinding Process, *Mater Res Expres.*, 2019, **6**(11), p 1165c9

9. K. Kishore, M.K. Sinha, A. Singh, Archana, M.K. Gupta, and M.E. Korkmaz, A Comprehensive Review on the Grinding Process: Advancements, Applications and Challenges, *Proc. Inst. Mech.. Eng. Part C J. Mech. Eng. Sci.*, 2022, **2022**, p 095440622211107. https://doi.org/10.1177/09544062221110782

10. T. Yu, X. Guo, Z. Wang, P. Xu, and J. Zhao, Effects of the Ultrasonic Vibration Field on Polishing Process of Nickel-Based Alloy Inconel718, *J. Mater. Process. Technol.*, 2019, **273**, p 116228

11. D. Bhaduri, S.L. Soo, D.K. Aspinwall, D. Novovic, S. Bohr, P. Harden, and J.A. Webster, Ultrasonic Assisted Creep Feed Grinding of Gamma Titanium Aluminide Using Conventional and Superabrasive Wheels, *CIRP Ann.*, 2017, **66**(1), p 341–344

12. A. Chaudhari, A. Sharma, A.S. Awale, M.Z.K. Yusufzai, and M. Vashista, Effect of Ultrasonic Vibration Assisted Dry Grinding on Hysteresis Loop Characteristics of AISI D2 Tool Steel, *Sadhana Acad. Proc. Eng. Sci.*, 2021, **46**(4), p 1–12. https://doi.org/10.1007/S12046-021-01771-5/FIGURES/12

13. H. Wang, Y. Hu, W. Cong, Z. Hu, and Y. Wang, A Novel Investigation on Horizontal and 3D Elliptical Ultrasonic Vibrations in Rotary Ultrasonic Surface Machining of Carbon Fiber Reinforced Plastic Composites, *J. Manuf. Process.*, 2020, **52**, p 12–25

14. Z. Yang, L. Zhu, B. Lin, G. Zhang, C. Ni, and T. Sui, The Grinding Force Modeling and Experimental Study of ZrO2 Ceramic Materials in Ultrasonic Vibration Assisted Grinding, *Ceram. Int.*, 2019, **45**(7), p 8873–8889

15. P.V. Badiger, V. Desai, M.R. Ramesh, B.K. Prajwala, and K. Raveendra, Effect of Cutting Parameters on Tool Wear, Cutting Force and Surface Roughness in Machining of MDN431 Alloy Using Al and Fe Coated Tools, *Mater. Res. Express*, 2019, **6**(1), p 016401

16. P.V. Badiger, V. Desai, M.R. Ramesh, B.K. Prajwala, and K. Raveendra, Cutting Forces, Surface Roughness and Tool Wear Quality Assessment Using ANN and PSO Approach During Machining of MDN431 with TiN/AlN-Coated Cutting Tool, *Arab. J. Sci. Eng.*, 2019, **44**(9), p 7465

17. P.V. Badiger, V. Desai, M.R. Ramesh, S. Joladarashi, and H. Gourkar, Tribological Behaviour of Monolayer and Multilayer Ti-Based Thin Solid Films Deposited on Alloy Steel, *Mater. Res. Express*, 2019, **6**(2), p 026419

18. P.V. Badiger, V. Desai, and M.R. Ramesh, Development and Characterization of Ti/TiC/TiN Coatings by Cathodic Arc Evaporation Technique, *Trans. Indian Inst. Met.*, 2017, **70**(9), p 2459

19. L. Zheng, W. Chen, and D. Huo, Review of Vibration Devices for Vibration-Assisted Machining, *Int. J. Adv. Manuf. Technol.*, 2020, **108**(5–6), p 1631–1651. https://doi.org/10.1007/S00170-020-05483-8/FIGURES/12

20. M. Dogra, V.S. Sharma, J.S. Dureja, and S.S. Gill, Environment-Friendly Technological Advancements to Enhance the Sustainability in Surface Grinding- A Review, *J. Clean. Prod.*, 2018, **197**, p 218–231

21. B. Azarhoushang, and T. Tawakoli, Development of a Novel Ultrasonic Unit for Grinding of Ceramic Matrix Composites, *Int. J. Adv. Manuf. Technol.*, 2011, **57**(9–12), p 945–955

22. H. Chen, and J. Tang, Influence of Ultrasonic Assisted Grinding on Abbott-Firestone Curve, *Int. J. Adv. Manuf. Technol.*, 2016, **86**(9–12), p 2753–2757

23. H. Chen, J. Tang, W. Shao, and B. Zhao, An Investigation on Surface Functional Parameters in Ultrasonic-Assisted Grinding of Soft Steel, *Int. J. Adv. Manuf. Technol.*, 2018, **97**(5–8), p 2697–2702

24. A. Abdullah, M. Sotoodezadeh, R. Abedini, and V. Fartashvand, Experimental Study on Ultrasonic Use in Dry Creep-Feed up-Grinding of Aluminum 7075 and Steel X210Cr12, *Int. J. Precis. Eng. Manuf.*, 2013, **14**(2), p 191–198

25. H. Chen, J. Tang, W. Shao, and B. Zhao, An Investigation on Surface Functional Parameters in Ultrasonic-Assisted Grinding of Soft Steel, *Int. J. Adv. Manuf. Technol.*, 2018, **97**(5), p 2697–2702. https://doi.org/10.1007/S00170-018-2164-X

26. H.C. Mult, G. Spur, and S.E. Holl, Ultrasonic Assisted Grinding of Ceramics, *J. Mater. Process. Technol.*, 1996, **62**(4), p 287–293

27. D. Li, J. Tang, H. Chen, and W. Shao, Study on Grinding Force Model in Ultrasonic Vibration-Assisted Grinding of Alloy Structural Steel, *Int. J. Adv. Manuf. Technol.*, 2019, **101**(5–8), p 1467–1479

28. X. Zhang, R. Huang, K. Liu, A.S. Kumar, and H. Deng, Suppression of Diamond Tool Wear in Machining of Tungsten Carbide by Combining Ultrasonic Vibration and Electrochemical Processing, *Ceram. Int.*, 2018, **44**(4), p 4142–4153

29. W.X. Xu, and L.C. Zhang, Ultrasonic Vibration-Assisted Machining: Principle, Design and Application, *Adv. Manuf.*, 2015, **3**(3), p 173–192

30. K. Ding, Y. Fu, H. Su, H. Xu, F. Cui, and Q. Li, Experimental Studies on Matching Performance of Grinding and Vibration Parameters in Ultrasonic Assisted Grinding of SiC Ceramics, *Int. J. Adv. Manuf. Technol.*, 2017, **88**(9–12), p 2527–2535

31. A. Awale, A.K. Shrivastava, A. Chaudhari, M. Vashista, and M.Z.K. Yusufzai, Micro-Magnetic Characterisation of Ground AISI D2 Tool Steel Using Hysteresis Loop Technique, *Int. J. Mater. Prod. Technol.*, 2021, **62**(1–3), p 180–198

32. K. Ding, Y. Fu, H. Su, X. Gong, and K. Wu, Wear of Diamond Grinding Wheel in Ultrasonic Vibration-Assisted Grinding of Silicon Carbide, *Int. J. Adv. Manuf. Technol.*, 2014, **71**(9), p 1929–1938. https://doi.org/10.1007/S00170-014-5625-X

33. A.S. Awale, A. Srivastava, M. Vashista, and M.Z. Khan Yusufzai, Influence of Minimum Quantity Lubrication on Surface Integrity of Ground Hardened H13 Hot Die Steel, *Int. J. Adv. Manuf. Technol.*, 2018, **100**(1), p 983–997. https://doi.org/10.1007/S00170-018-2777-0

34. M.K. Sinha, "Experimental Investigations in Grinding of Inconel 718 Using Different Environments and Modelling of Specific Grinding Energy. Doctoral Dissertation IIT Delhi, 2018. ," (New Delhi), Indian Institute of Technology Delhi, 2018, http://www.eprint.iitd.ac.in/handle/2074/7536. Accessed 8 August 2022

35. I.D. Marinescu, W. Brian Rowe, B. Dimitrov, and H. Ohmori, Tribosystems of Abrasive Machining Processes, *Tribology of Abrasive Machining Processes*. Elsevier, 2013

36. S. Das, and C. Pandivelan, Grinding Characteristics during Ultrasonic Vibration Assisted Grinding of Alumina Ceramic in Selected Dry and MQL Conditions, *Mater. Res. Express*, 2020, **7**, p 85404. https://doi.org/10.1088/2053-1591/abad14

37. A. Sharma, A. Chaudhari, A.S. Awale, M.Z.K. Yusufzai, and M. Vashista, Effect of Grinding Environments on Magnetic Response of AISI D2 Tool Steel, *Russ. J. Nondestruct. Test.*, 2021, **57**(3), p 212–221

38. A.S. Awale, A. Chaudhari, A. Kumar, M.Z. Khan Yusufzai, and M. Vashista, Synergistic Impact of Eco-Friendly Nano-Lubricants on the Grindability of AISI H13 Tool Steel: A Study towards Clean Manufacturing, *J. Clean. Prod.*, 2022, **364**, p 132686

39. S. Lou, Z. Zhu, W. Zeng, C. Majewski, P.J. Scott, and X. Jiang, Material Ratio Curve of 3D Surface Topography of Additively Manufactured Parts: An Attempt to Characterise Open Surface Pores, *Surf. Topogr. Metrol. Prop.*, 2021, **9**(1), p 015029. https://doi.org/10.1088/2051-672X/ABEDF9

40. P. He, S. Lu, Y. Wang, R. Li, and F. Li, Analysis of the Best Roughness Surface Based on the Bearing Area Curve Theory, *Proc. Inst. Mech. Eng. Part J J. Eng. Tribol.*, 2021, **236**(3), p 527–540. https://doi.org/10.1177/13506501211018937

41. M. Jamshidinia, and R. Kovacevic, The Influence of Heat Accumulation on the Surface Roughness in Powder-Bed Additive Manufacturing, *Surf. Topogr. Metrol. Prop.*, 2015, **3**(1), p 014003. https://doi.org/10.1088/2051-672X/3/1/014003

Publisher's Note Springer Nature remains neutral with regard to jurisdictional claims in published maps and institutional affiliations.